Relief Reconstruction from SAR Stereo Pairs: The "Optimal Gradient" Matching Method

Philippe PAILLOU
Université de Bordeaux 3, avenue des Facultés, 33405 Talence Cedex, France
tel: (33) 5 56 84 80 71 fax: (33) 5 56 84 80 73 e-mail: phi@egid.u-bordeaux.fr
Margrit GELAUTZ
Institute for Computer Vision and Graphics - Technical University Graz
Muenzgrabenstrasse 11, A-8010 Graz, Austria
tel: (43) 316 873 5031 fax: (43) 316 873 5050 e-mail: gelautz@icg.tu-graz.ac.at

Abstract **- We present a method for improving relief reconstruction from SAR stereo images, relying on pre-processing of input data with an optimal filter. This filter strongly reduces speckle noise and enhances relief structures, leading to better matching results. The method was tested using X-SAR data of a mountainous site whose DEM was available for control.**

I. INTRODUCTION

A classical method for relief reconstruction using remote sensing images is stereogrammetry. This technique can be applied to SAR stereo data, allowing the production of good quality digital elevation models (DEM) [Leberl 90]. The core process here is stereo matching, that is finding disparity - or correspondence points - between two images acquired from different sensor positions. This can be done manually (more or less computer-aided) [Toutin 95] or automatically [Leberl 94]. The main problem when performing stereo matching is the need for some image disparity in order to reconstruct relief, but not too much so that enough correspondence points can still be found. These contradictory requirements are encountered when dealing with optical data, however the problem is more pronounced when one considers radar images that can be very different when incidence angle changes (for strong relief regions). This difficulty exists for same-side viewing geometry and is stronger for opposite-side geometry [Toutin 96] where the geometric and radiometric image disparity can be so high that even the manual matching process can fail.

Most automated matching methods rely on correlation between images in order to produce a disparity map. Matching can be performed using initial grey level images [Ramapriyan 86], edge images [Pratt 74], or some other image features such as linked-edge elements or regions [Flusser 94]. The correlation algorithm can be improved by the use of hierarchical image representation [Cohen 89] and combining multiple image primitives [Marapane 94]. New methods based on learning process [Lew 94] or wavelet transform [Djamdji 95] for instance were also proposed. The success of all these methods, more or less complicated, depends on the information quality contained in input stereo images: even a complex method can fail with noisy and badly structured input data, whereas a simple correlation technique may give good results when dealing with suitable input data. This data-dependency also limits the applicability of matching algorithms, which were originally designed for optical imagery to their radar counterpart. In particular, the combination of so-called feature based (using image features such as edges or corners) and correlation based methods has already been applied successfully in optical image matching [Zhang 95]. Contrarily, the existing literature on radar image matching has been generally limited to basic correlation of image grey values. The main problems encountered when matching SAR images, as opposed to optical data, are speckle noise and that the two stereo partners can be very different from one another, as the backscattered radar signal mainly depends on the local incidence angle. In particular, for opposite side stereo pairs or same side stereo pairs with very large intersection angle, the so-called specular-point migration effect [Curlander 91] can cause problems since dominant scatterers identified in both images are not always representative of the same ground feature. Other geometrical effects such as layover and shadows can also disturb the correlation process [Gelautz 97]. The study of such extreme cases is out of the scope of this paper: we deal here with same side stereo pairs and low intersection angle, and radar images processed do not present layover effects.

We propose here to improve the image matching process using a specific pre-processing of input stereo pair. This pre-processing reduces speckle noise from SAR data and strongly enhances image structures that are then further used within the matching process. The input SAR stereo pair is processed using an optimal filter [Paillou 97a] that is very efficient for radar images. This filter produces gradient amplitude like images that are used as input for registration. Gradient amplitude images are then automatically matched utilizing an available correlation based algorithm [Hensley 94]. This so-called "Optimal Gradient" Matching - OGM - method is described in section II. Experimental results are presented in section III: we first used X-SAR same-side viewing stereo images together with a reference DEM in order to validate our method and to show that better results are obtained

compared to the use of initial SAR images. The technique was then applied to relief reconstruction of Venus surface from Magellan mission data.

II. GRADIENT STEREOGRAMMETRY

The classical approach in radar stereogrammetry is based on image matching using correlation methods in order to generate a disparity map that is then converted into a height map or DEM. This technique suffers from an internal contradiction: the two stereo images must be different enough so that the relief effect occurs (relative displacement of image structures) but this difference (dissimilarity) between images must not be too big in order to be able to perform image matching. While good results are obtained with classical images (using SPOT stereo pairs for instance), the use of SAR images presents some particular difficulties: dissimilarity between radar images can be important due to illumination effects and SAR images present high noise level that disturbs the matching process.

These difficulties can be overcome to a certain extent if we consider some limitations: use of same-side stereo data with small intersection angle, relief reconstruction for smooth relief areas (provided that in the absence of topographic features enough texture is still present due to thematic variation), use of reference correspondence points, use of hierarchical matching methods, SAR image filtering for noise reduction, etc. A further possibility would be to employ a feature-based approach, which performs matching using image structures rather than grey value images. In particular, we can consider that edges contained in images are good descriptors for image structures and are more invariant than original pixel grey levels, thus allowing the use of more dissimilar stereo pairs. We assume here that edges in both images of the stereo pair are only due to relief structures and represent the same ground feature.

We use here as input for the matching process images obtained from a linear optimal gradient operator. This operator was designed to be optimal with respect to noise removal - that is crucial when dealing with radar images - and it strongly enhances the image structures due to relief. Furthermore, edges - that is local gradient amplitude maxima - contained in images proved to be more similar than original grey values, allowing better results for the matching process. It has to be remarked that we are dealing here with gradient amplitude images - that is *all pixels* of the images are used for matching - and not with edge images where only gradient amplitude local maxima - that is a few pixels - are taken into account.

Experimental results of the OGM method are presented below. They show that the use of gradient amplitude images produced by our optimal filter improves the relief reconstruction process. As this improvement only relies on pre-processing of input stereo images, it is not directly related to the matching process itself that in principle can be freely chosen.

A. Gradient Amplitude Images

Several differentiation-based gradient operators were developed (see for instance [Canny 86, Deriche 89, Shen 92]), associating edges in image to local maxima of the gradient amplitude. When dealing with SAR images that are very noisy, one should consider an operator with very low sensitivity to noise. We derived a gradient operator that allows to obtain very high insensitivity to noise and that can be recursively implemented. Results obtained using this filter show better performances than other classical differential operators [Paillou 97a].

Let us consider a one-dimensional signal to be processed $I(x)$ (e.g. an image row). The one-dimensional filter $f(x)$ used is an hyperbolic sinus form expressed by:

$$f(x) = -ce^{-\alpha|x|}\sin(\omega x), \qquad \text{with } c,\alpha,\omega \text{ reals} > 0 \tag{1}$$

Taking $\omega/\alpha \rightarrow 1$ allows very good filter performances with respect to signal to noise ratio (see [Paillou 97a] for details). Gradient amplitude of $I(x)$ is obtained by convoluting the input signal $I(x)$ with the anti-symmetrical function $f(x)$. Edges are located at maxima of the result of convolution $O(x_0)$ given by:

$$O(x_0) = \int_{-\infty}^{+\infty} I(x)\, f(x_0 - x)dx \tag{2}$$

No localization error - that is edge displacement that could be interpreted as a stereoscopic effect - is produced by this filter when dealing with antisymmetrical edge profiles [Paillou 94], which is normally the case for relief structures in radar images.

From this filter, we derived two two-dimensional directional masks $X(i,j)$ and $Y(i,j)$ that are convoluted with each input SAR image $I(x,y)$. We then obtain respectively an $I_X(i,j)$ and an $I_Y(i,j)$ image. The gradient amplitude image $A(i,j)$ and the gradient direction image $D(i,j)$ are given by the following relationships:

$$A(i,j) = \sqrt{I_x^2(i,j) + I_y^2(i,j)} \qquad D(i,j) = \tan^{-1}\left(\frac{I_y(i,j)}{I_x(i,j)}\right) \tag{3}$$

This filter was applied to noisy SAR images presented in Fig. 1a, Fig. 1b, and Fig. 5a, Fig. 5b. Obtained gradient amplitude images are shown in Fig. 1c, Fig. 1d, and Fig. 5c, Fig. 5d. Gradient amplitude images show bright zones where SAR image brightness changes occur. As expected, this pre-processing greatly reduced speckle noise and enhanced image structures that can be further used within the registration process. Furthermore, when considering stereo pairs, gradient amplitude images are more similar than original SAR images as will be shown in section III.

B. The Matching Process

In order to perform gradient amplitude image matching, we employed a hierarchical approach based on a two-dimensional normalized cross-correlation [Hensley 94]. Registration is performed on four successively finer scales, using matching templates of 64 x 64, 32 x 32, 16 x 16, and 8 x 8 image pixels. A local polynomial warping function between the stereo image pair is used to predict offsets at the next level of the hierarchical process. At each resolution level, a cross-correlation is carried out, and the shape of the correlation surface along with a local scene noise estimate is then used to compute a confidence value for the corresponding match point. This confidence measure is a two-dimensional covariance matrix which reflects the directional reliability of the matching result. It can be utilized to filter out bad matches and to forward error information to the DEM reconstruction process.

In our tests, the correlation software was run with the suggested default values; the same set of parameters was employed for matching the original and pre-processed image pairs. In order to compensate for the missing match points and to fill in the pixels in between the 8 x 8 grid, we then had to use interpolation techniques to generate the final disparity map. We used a kriging interpolation method with a gaussian variogram model. Some smoothing was performed through a nugget effect [Cressie 91].

The reconstructed DEM is obtained from the interpolated disparity map using the relationship [Leberl 90]:

$$h = \frac{d}{\cot(\theta_{2i}) - \cot(\theta_{1i})} \tag{4}$$

where h is the height of the relief feature of parallax (disparity) d, and θ_{1i} and θ_{2i} are the incidence angles of the two stereo partners for the i^{th} pixel in range line. Although this formula is based on the assumptions of parallel and same altitude flights over a flat terrain, we take into account the satellite height variations and planetary surface curvature by computing local incidence angles for each line pixel [Ansan 95]. We can consider parallel flight lines for X-SAR images since the angle difference is about 1.6 degree and we work with small image segment parts.

Finally, the reconstructed DEM is projected into a given geographical system for comparison with a reference digital elevation map. Residual height mean error is removed from the reconstructed DEM using control points taken into the reference digital elevation map (when available). It allows us to remove systematic errors due to uncertainty of geometrical model, satellite orbit parameters and reference DEM. We shall then focus on height error standard deviation.

III. EXPERIMENTAL RESULTS

Results presented here are within the scope of a comparative study of venusian and terrestrial rift zones using radar remote sensing [Paillou 97b]. This study aims at obtaining quantitative data about Venus surface relief and geological nature from SAR images. A terrestrial test site located in the Austrian Alps was used to evaluate the proposed method performances. We then applied it to relief reconstruction of Venus surface.

A. Terrestrial site

Our test site is the Oetztal, a rugged terrain in the Austrian Alps with elevations ranging from 1750 m to more than 3750 m [Gelautz 96]. It was imaged by SIR-C/X-SAR mission in April 1994 and we processed an X-band stereo pair with respectively 58.1° and 50.3° incidence angles, and 25m x 25m pixel size (see Fig. 1a and Fig. 1b). Each image contains 512 x 512 pixels. In order to evaluate our method performances, we compared our results to a reference digital elevation model of the Oetztal site (pixel size 25m x 25m) presented in Fig. 2a and Fig. 2b. This reference DEM was obtained by digitizing contour lines of topographic maps in a scale of 1:25000, with a global accuracy of about 5 meters rms error. Because the disparity map was obtained by interpolation of a 8 x 8 pixels match points grid, we reduced our reference DEM resolution (see Fig. 2c and Fig. 2d) so that it can be compared to

the stereo process result.

Fig. 3a and 3b show the reconstructed DEM using initial SAR images, while Fig. 3c and 3d present the reconstructed DEM using gradient amplitude images. These results have to be compared to Fig. 2c and 2d. The two DEMs look very similar at first glance, but quantitative analysis of some selected areas shows that the use of gradient amplitude images as input produced a better result.

Fig. 4 presents a comparison between reconstructed DEMs in Fig. 3a and 3c, and the ground truth in Fig. 2c. Four areas of size 128 x 128 pixels were selected to build difference images between each computed DEM and the reference DEM. These areas correspond to regions where highest differences between computed and reference DEMs can be seen. Height and slope statistics for the four selected zones were obtained from the 25m resolution reference DEM and are presented in Table I. We present in Fig. 4a to Fig. 4d error histograms for the four corresponding difference images. One can see that the reconstruction error related to the proposed OGM method is smaller than the error related to the use of original SAR images: we can see more points around zero meter error (histogram center) and fewer points for large error values (histogram wings), in particular for zone #2. This is confirmed by computed error means and standard deviation presented in Table II. In particular, the error dispersion and the maximum error are in all cases much smaller for the OGM method.

Comparing Tables I and II shows that the error dispersion increases as the mean slope and height standard deviation becomes larger: this effect could be due to higher shadow effects leading to "non-relief edges" in high slope regions. We used a simulated shadow map to examine the effects of shadow boundaries on the features in the gradient amplitude image and found that in our imagery the migrating far range boundaries were mainly located at the rather smooth transition between shadows and (still dark) regions facing away from the sensor. They thus lead to only weak structures in the gradient amplitude image, with less influence on the matching process. If a far range shadow boundary borders directly on a (bright) foreshortened region, the higher contrast of the non-relief edge will perturbate the subsequent correlation more. The lack of relief information inside a shadow region would be a further possible source of error. We did not analyse these effects in detail, which is beyond the scope of the paper. However, they could increase the reconstruction error: we observed that this error increases as the mean slope and height standard deviation of the considered zone increases (see Tables I and II), which seems to be correlated to the shadow percentage. On the other hand, the rather high percentage of shadows found in zone #4, compared to the corresponding mean slope and height standard deviation values, is not reflected in the error statistics. This might indicate a stronger influence of terrain roughness rather than shadows on height accuracy.

B. Venus surface

The US mission Magellan [Saunders 92] provided a huge amount of SAR images of the venusian surface, together with altimetry, reflectivity and emissivity data. The whole surface was imaged in S-band with a mean resolution of 120 meters. Here, the main problem in extracting quantitative information from images is the lack of ground truth data needed to calibrate theoretical models and image processing techniques. A solution to overcome that difficulty is the use of known comparable terrestrial sites for model calibration [Campbell 94].

One stereo pair from the Magellan stereo experiment [Leberl 92] was processed: Fig. 5 shows a venusian impact crater with its central peak located 5^{o}S-76^{o}E that was obtained from imaging cycle 1 (43.8^{o} incidence angle, see Fig. 5a) and cycle 3 (24.9^{o} incidence angle, see Fig. 5b). As expected for large intersection angles, some relief structures are very dissimilar in the two stereo images: see for instance the crater central peak in Fig. 5a and 5b. As previously, we computed a DEM from initial SAR images (Figs. 6a and 6b) and from gradient amplitude images (Figs. 6c and 6d). Again, using our pre-processing filter produces the best result: no ground truth is here available for quantitative evaluation, but from comparison with Figs. 5a and 5b one can observe that the crater central peak is reconstructed much better in Fig. 6d than in Fig. 6b. We can also notice that the northern crater border break which can be seen in Figs. 5a and 5b only appears in Figs. 6c and 6d. These two features - crater central peak and northern border break - appear very well when using classical stereo viewing techniques.

IV. CONCLUSION

We proposed a method that improves relief reconstruction from SAR stereo imaging, based on the use of gradient amplitude images. Our method relies on pre-processing the initial SAR stereo pair using an optimal gradient filter with respect to insensitivity to noise. It reduces speckle noise in SAR images and enhances the image structures that are then used in the matching process. Experimental results obtained using JPL radar matching software show that the proposed filtering produces better results than using original non-enhanced SAR images. As the improvement only depends on the pre-processing stage, the method can also be applied in combination with other matching technique. Application of this gradient method to opposite-side stereo imaging is currently under study.

ACKNOWLEDGMENTS

The authors wish to thank Scott Hensley from NASA/JPL for providing his matching software. Further thanks go to Dr. Philippe Masson from the University of Paris-Sud and Dr. Helmut Rott from the University of Innsbruck for making available the Magellan mission and X-SAR data, respectively. We are also grateful to the anonymous reviewers for their constructive remarks.

REFERENCES

[Ansan 95] V. Ansan, *Creating digital elevation models from stereoscopic SAR images*, CNES Technical Report 961/CNES/93/0975/00, 1995.

[Canny 86] J. F. Canny, "A computational approach to edge detection," *IEEE Transactions on Pattern Analysis and Machine Intelligence*, vol. 8, 1986.

[Campbell 94] B. A. Campbell, P. G. Rogers, "Bell Regio, Venus: Integration of remote sensing data and terrestrial analogs for geologic analysis," *JGR-Planets*, vol. 99, pp. 21153-21171, 1994.

[Cohen 89] L. Cohen, L. Vinet, P. Sander, "Hierarchical region based stereo matching," *Proc. IEEE Conf. on Computer Vision and Pattern Recognition*, pp. 416-421, 1989.

[Cressie 91] N. A. Cressie, *Statistics for Spatial Data*. New York: John Wiley and Sons Inc., 1991.

[Curlander 91] J. C. Curlander, R. N. McDonough, *Synthetic Aperture Radar: Systems and Signal Processing*, New York, J. Wiley and Sons Inc., 1991.

[Deriche 89] R. Deriche, "Fast algorithms for low-level vision," *IEEE Transactions on Pattern Analysis and Machine Intelligence*, vol. 12, 1989.

[Djamdji 95] J.-P. Djamdji, A. Bijaoui, "Disparity analysis: A wavelet transform approach," *IEEE Transactions on Geoscience and Remote Sensing*, vol. 33, no. 1, pp. 67-76, 1995.

[Flusser 94] J. Flusser, T. Suk, "A moment-based approach to registration of images with affine geometric distortion," *IEEE Transactions on Geoscience and Remote Sensing*, vol. 32, no. 2, pp. 382-387, 1994.

[Gelautz 96] M. Gelautz, G. Jakob, G. Paar, S. Hensley, F. Leberl, "Automated matching experiments with different kinds of SAR imagery," *Proc. IGARSS'96*, Lincoln, NE, pp. 31-33, 1996.

[Gelautz 97] M. Gelautz, *Integration of Layover Information into SAR Image Analysis*, Ph.D. Thesis, Technical University of Graz, Austria, 1997.

[Hensley 94] S. Hensley, S. Shaffer, "Automatic DEM generation using Magellan stereo data," *Proc. IGARSS'94*, Pasadena, CA, pp. 1470-1472, 1994.

[Leberl 90] F. W. Leberl, *Radargrammetric Image Processing*, Norwood, MA: Artech House Inc., 1990.

[Leberl 92] F. W. Leberl, J. K. Thomas, K. E. Maurice, "Initial results from the Magellan stereo experiment," *JGR-Planets*, vol. 97, pp. 13675-13689, 1992.

[Leberl 94] F. W. Leberl, K. Maurice, J. K. Thomas, M. Millot, "Automated radar image matching experiment," *ISPRS Journal of Photogrammetry and Remote Sensing*, vol. 49, no. 3, pp. 19-33, 1994.

[Lew 94] M. S. Lew, T. S. Huang, K. Wong, "Learning and feature selection in stereo imaging," *IEEE Transactions on Pattern Analysis and Machine Intelligence*, vol. 16, no. 9, pp. 869-881, 1994.

[Marapane 94], S. B. Marapane, M. M. Trivedi, "Multi-primitive hierarchical (MPH) stereo analysis," *IEEE Transactions on Pattern Analysis and Machine Intelligence*, vol. 16, no. 3, pp. 227-240, 1994.

[Paillou 94] Ph. Paillou, "Non-antisymmetrical edge profile detection," *Pattern Recognition Letters*, vol. 15, pp. 595-605, 1994.

[Paillou 97a] Ph. Paillou, "Detecting step edges in noisy SAR images: A new linear operator," *IEEE Transactions on Geoscience and Remote Sensing*, vol. 35, no. 1, pp. 191-196, 1997.

[Paillou 97b] Ph. Paillou, Ph. Masson, T. Souriot, "A comparative study of terrestrial rifts (Djibouti) and venusian rifts (Atla Regio) using radar remote sensing," *Int. Symp. on volcanism, rifting and paleoclimates in the Ethiopian rift and Afar depression*, Addis Abeba, Ethiopie, february 1997.

[Pratt 74] W. Pratt, "Correlation techniques of image registration," *IEEE Transactions on Aerospace and Electronic Systems*, vol. 10, pp. 353-358, 1974.

[Ramapriyan 86] H. K. Ramapriyan, J. P. Strong, Y. Hung, C. H. Murray, "Automated matching of pairs of SIR-B images for elevation mapping," *IEEE Transactions on Geoscience and Remote Sensing*, vol. GE-24, no. 4, pp. 462-472, 1986.

[Saunders 92] R. S. Saunders *et al*., "Magellan mission summary," *JGR-Planets*, vol. 97, pp. 13067-13090, 1992.

[Shen 92] J. Shen, S. Castan, "An optimal linear operator for step edge detection," *Computer Vision, Graphics and Image Processing*, vol. 54, 1992.

[Toutin 95] T. Toutin, "Airborne SAR stereo restitution in a mountainous area of Costa Rica: First results," *IEEE*

Transactions on Geoscience and Remote Sensing, vol. 33, no. 2, pp. 500-504, 1995.
[Toutin 96] T. Toutin, "Opposite side ERS-1 SAR stereo mapping over rolling topography," *IEEE Transactions on Geoscience and Remote Sensing*, vol. 34, no. 2, pp. 543-549, 1996.
[Zhang 95] Z. Zhang, R. Deriche, O. Faugeras, Q. Luong, "A robust technique for matching two uncalibrated images through the recovery of the unknown epipolar geometry," *Artificial Intelligence Journal*, vol. 78, pp. 87-119, 1995.

		Zone #1	Zone #2	Zone #3	Zone #4	Whole area
Height (meters)	**Min**	2378	2168	2179	2583	1871
	Max	3304	3206	3361	3498	3666
	Mean	2841	2755	2802	2999	2815
	Sdev	182	223	270	173	333
Slope (degrees)	**Min**	1	0	1	0	0
	Max	59	61	60	56	63
	Mean	25	24	30	24	27
	Sdev	9	10	11	11	11
Shadow	**percentage**	5.8	6.3	10.3	10.5	9.9

Table I. Height and slope statistics and computed shadow percentage for the four selected zones compared to the whole area (obtained from the 25m resolution reference DEM).

		Zone #1	Zone #2	Zone #3	Zone #4
OGM	**Mean**	0.17	0.16	0.17	0.18
	Sdev	43.45	43.51	47.92	32.95
	Max	117.17	139.08	126.70	89.87
SAR	**Mean**	0.17	0.17	0.18	0.18
	Sdev	46.65	49.10	60.73	40.49
	Max	134.67	173.51	163.94	131.65

Table II. Reconstruction error mean, standard deviation and maximum (in meters) for the four selected zones (OGM: relief reconstructed from gradient amplitude images, SAR: relief reconstructed for initial SAR images).

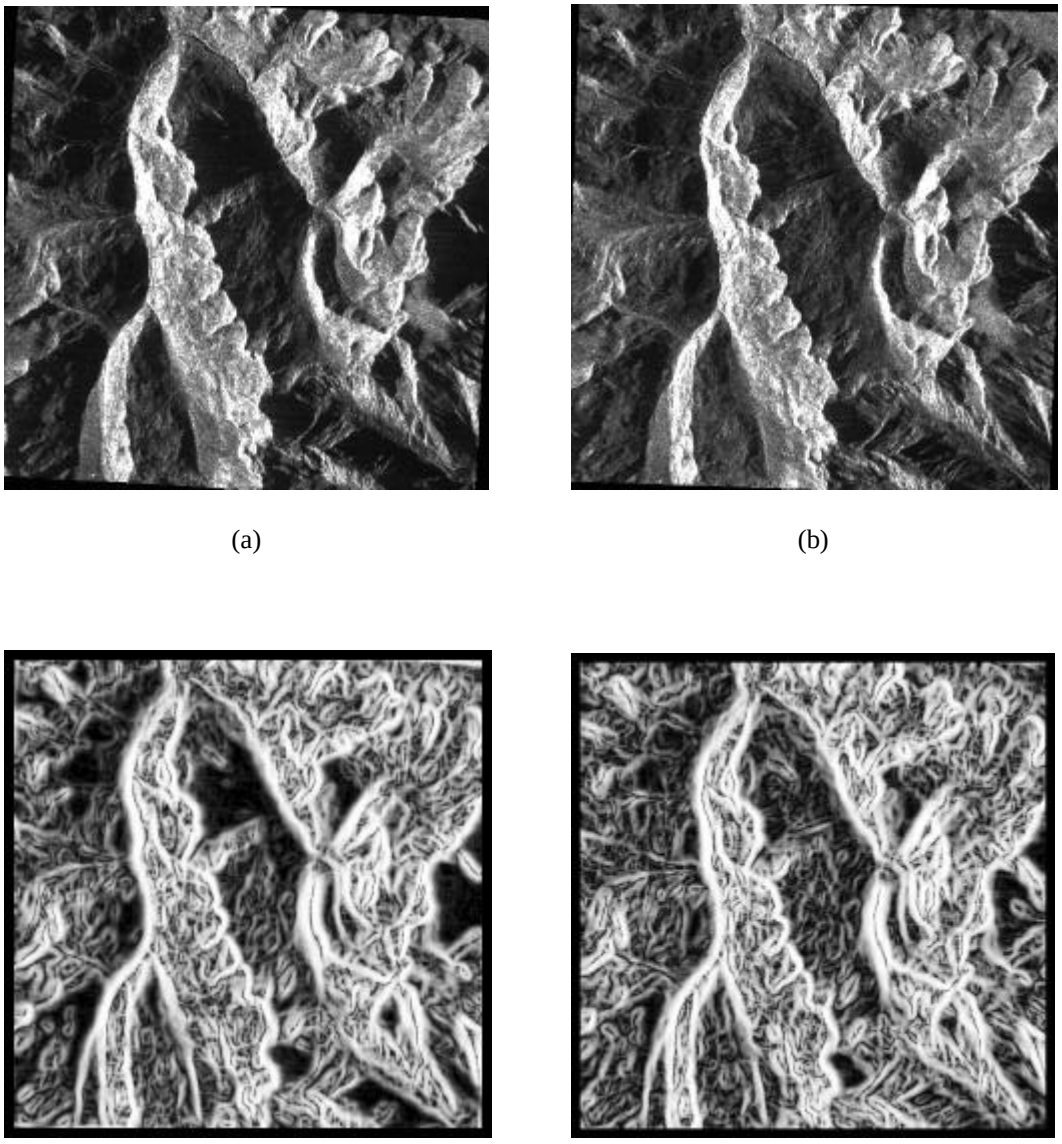

(a) (b)

(c) (d)

Fig. 1. Oetztal site as imaged by X-SAR X-band SAR in April 1994: (a) 58.1^o incidence angle and (b) 50.3^o incidence angle (the pixel size is 25m x 25m). Corresponding gradient amplitude images computed using our filter with α=1.0, ω=0.6: (c) 58.1^o incidence angle and (d) 50.3^o incidence angle.

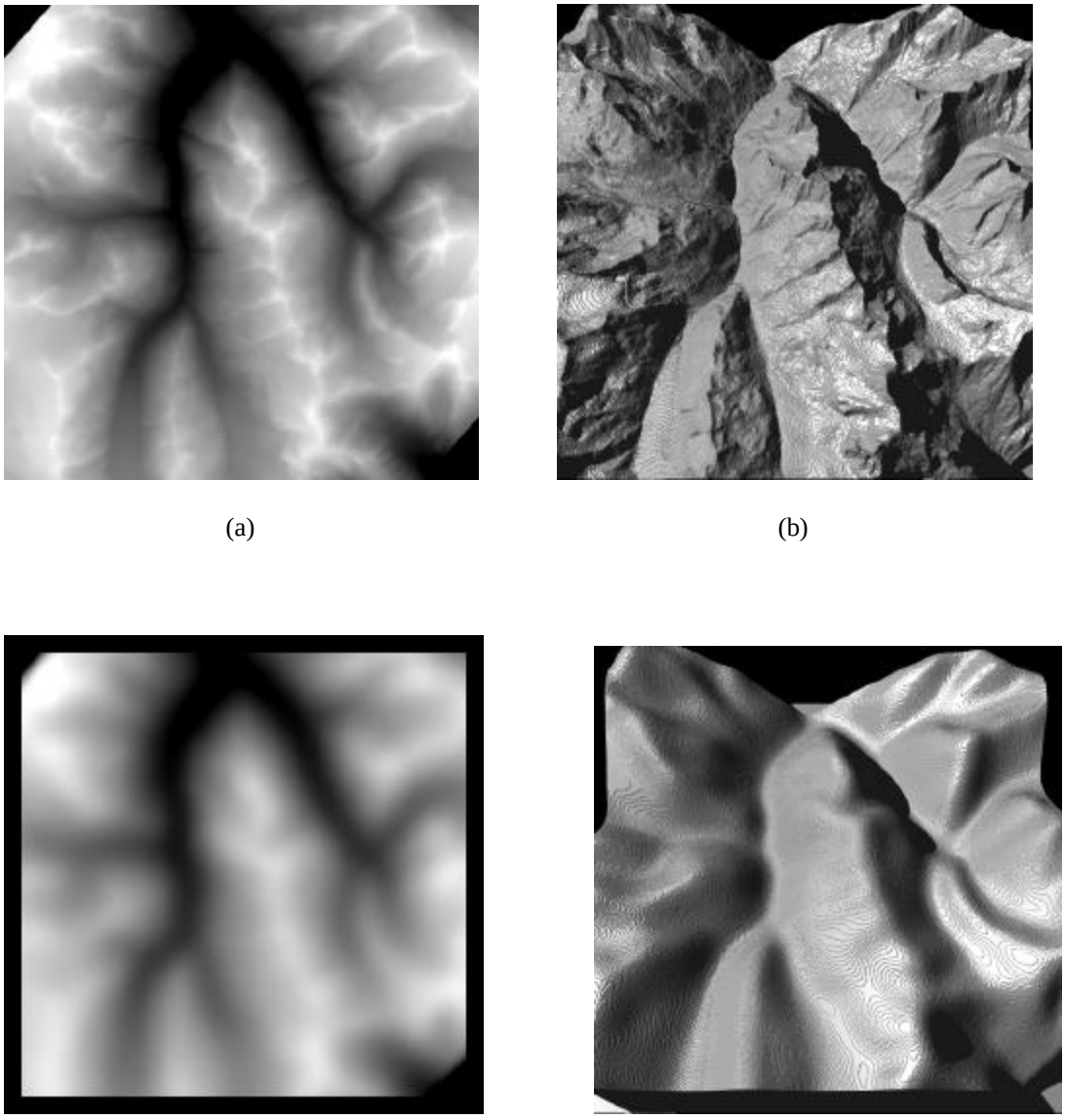

(a) (b)

(c) (d)

Fig. 2. Oetztal site digital elevation model, with pixel size 25 m x 25 m (a) and a corresponding perspective view (b). Same DEM with resolution reduced by a factor 8 (c) and its perspective view (d).

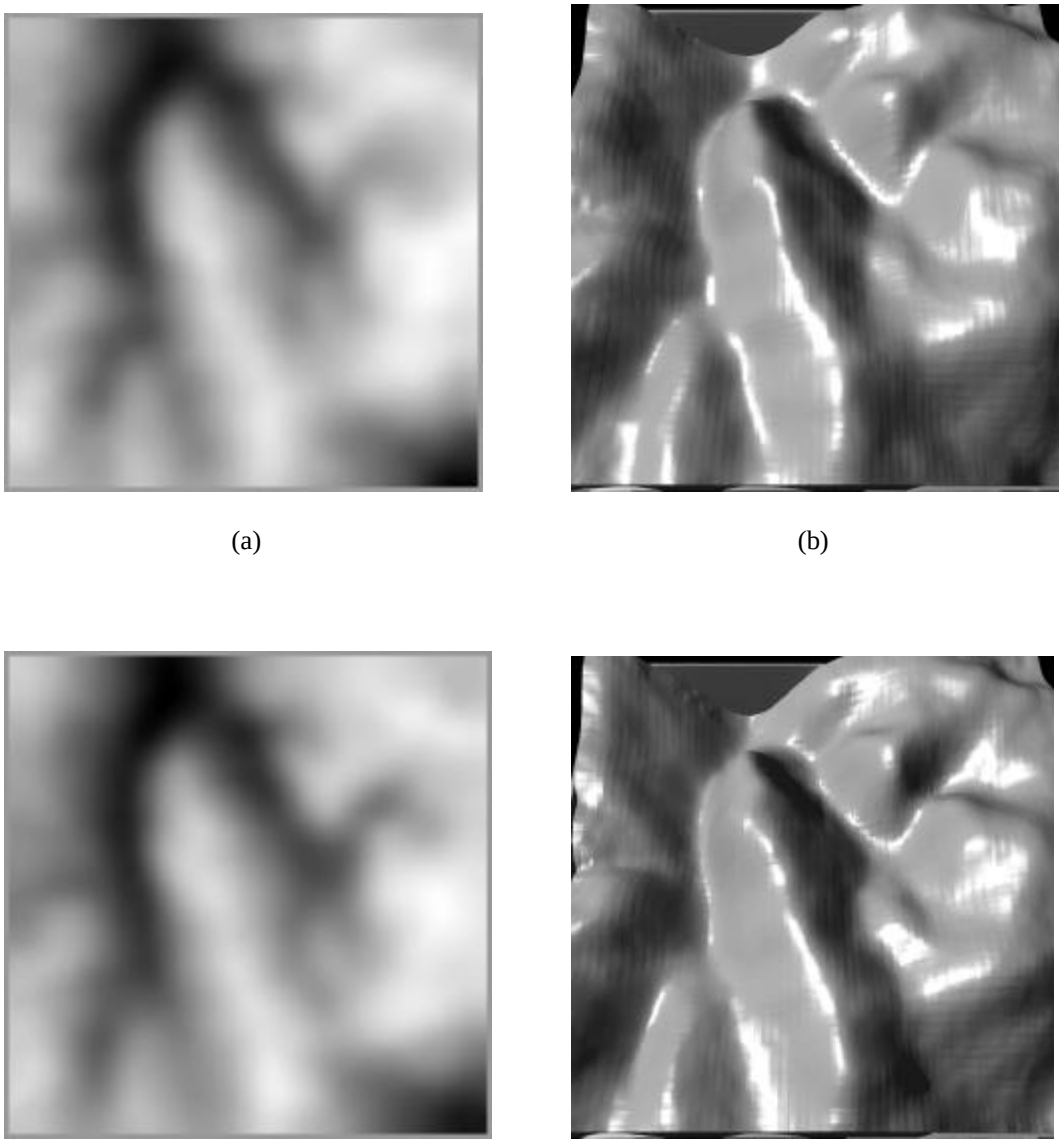

(a) (b)

(c) (d)

Fig. 3. Reconstructed DEM from initial X-SAR images - (a) and (b) - and from gradient amplitude images - (c) and (d).

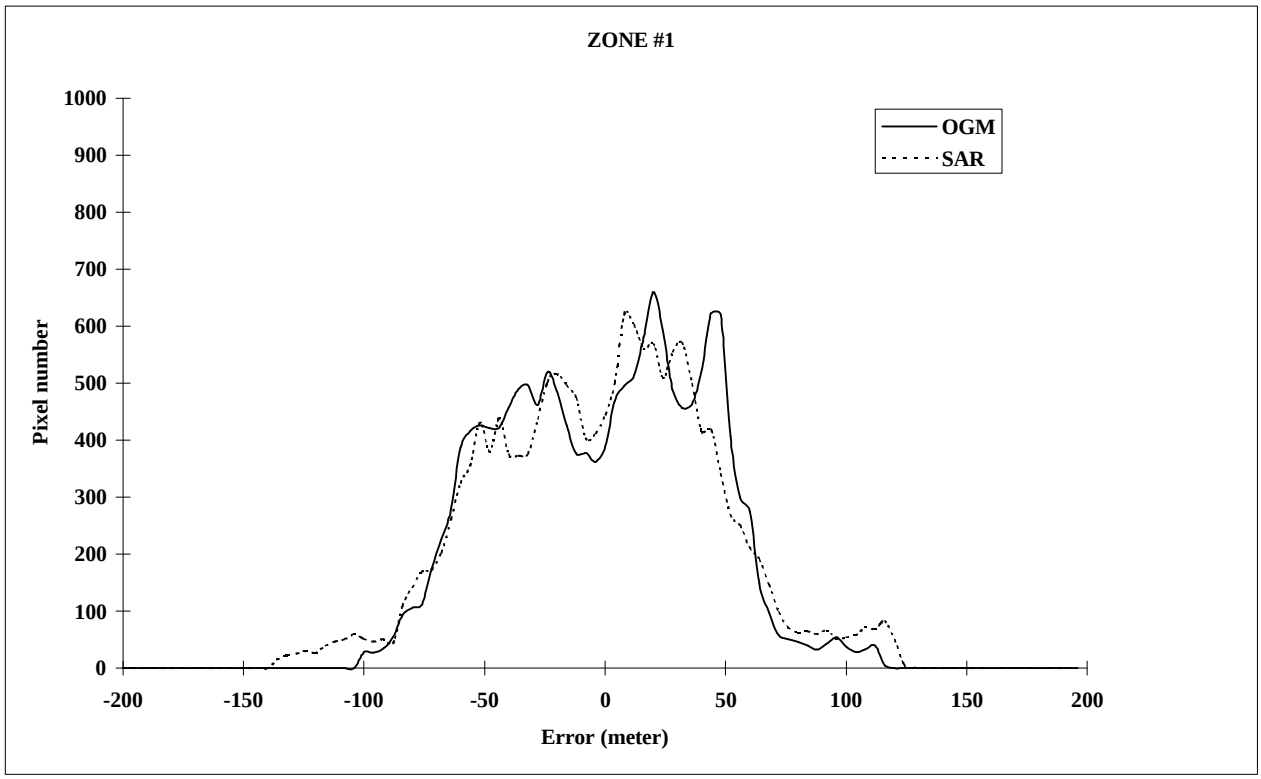

(a)

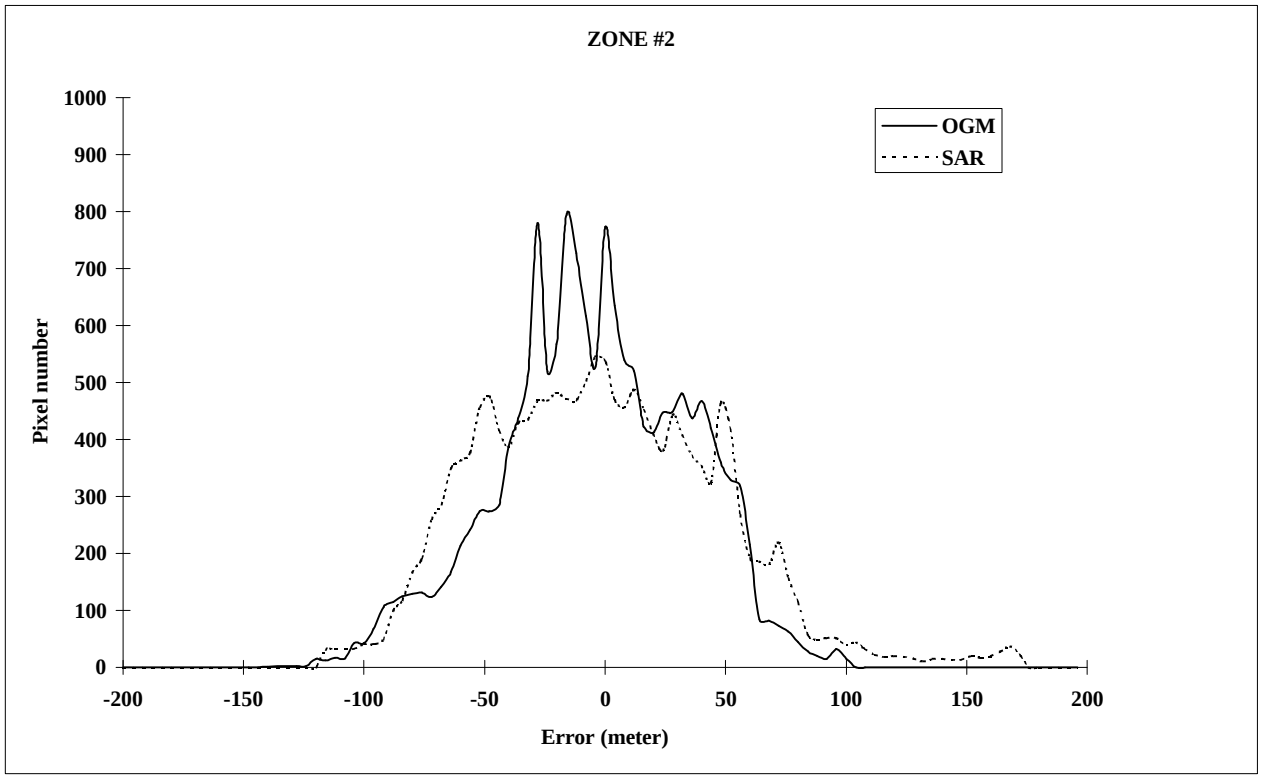

(b)

Fig. 4. Error histograms for zone #1 (a) and zone #2 (b).

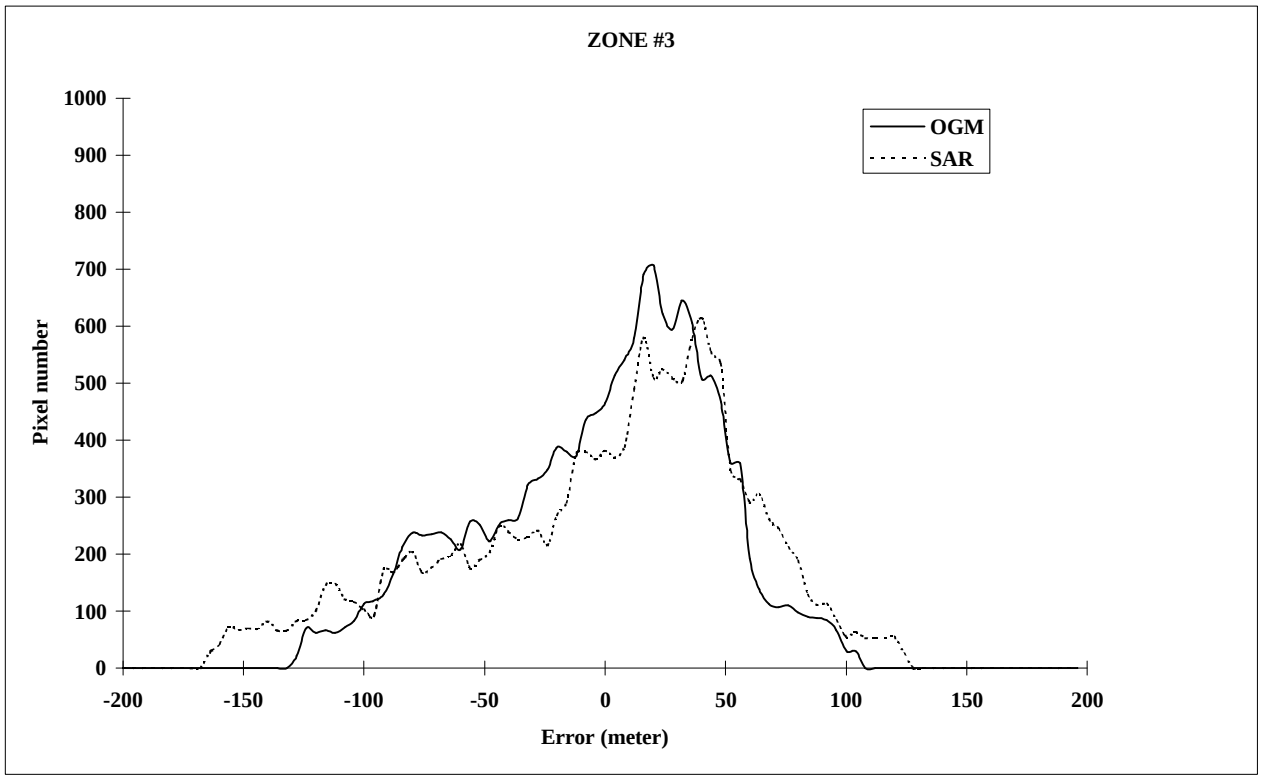

(c)

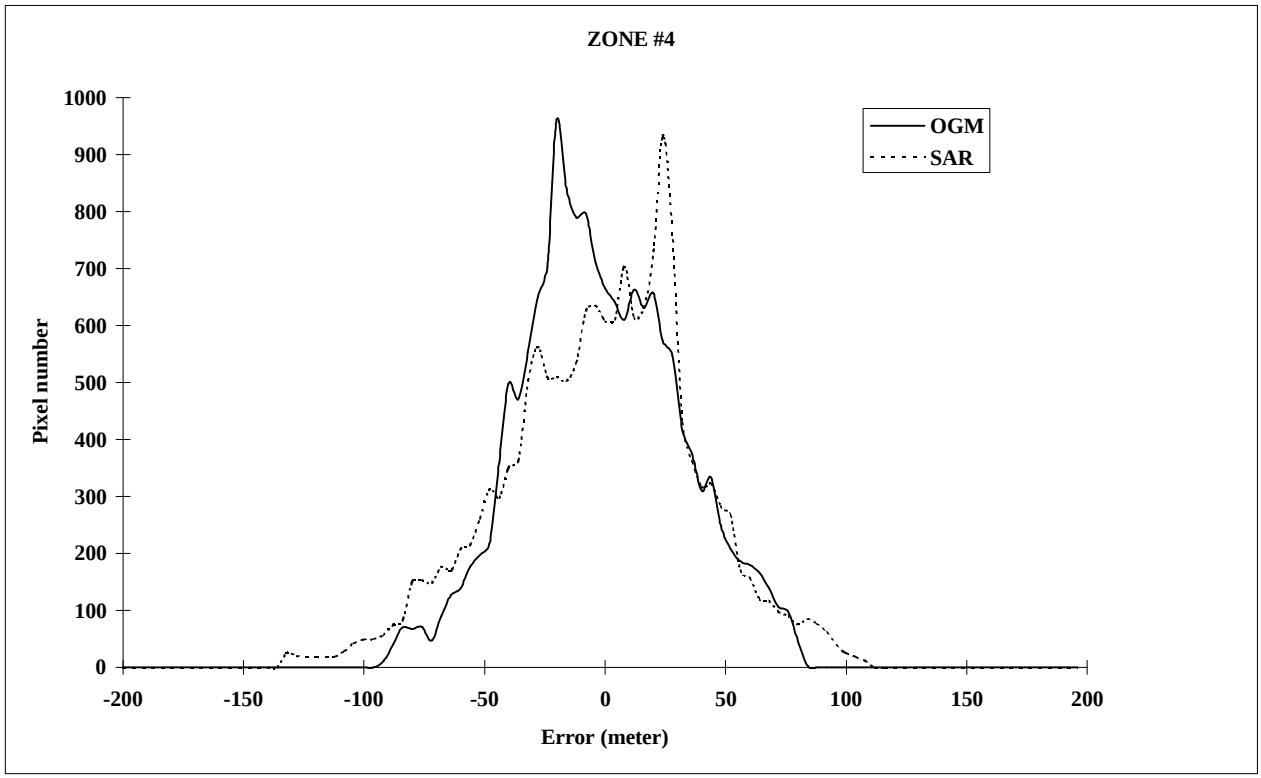

(d)

Fig. 4. Error histograms for zone #3 (c) and zone #4 (d).

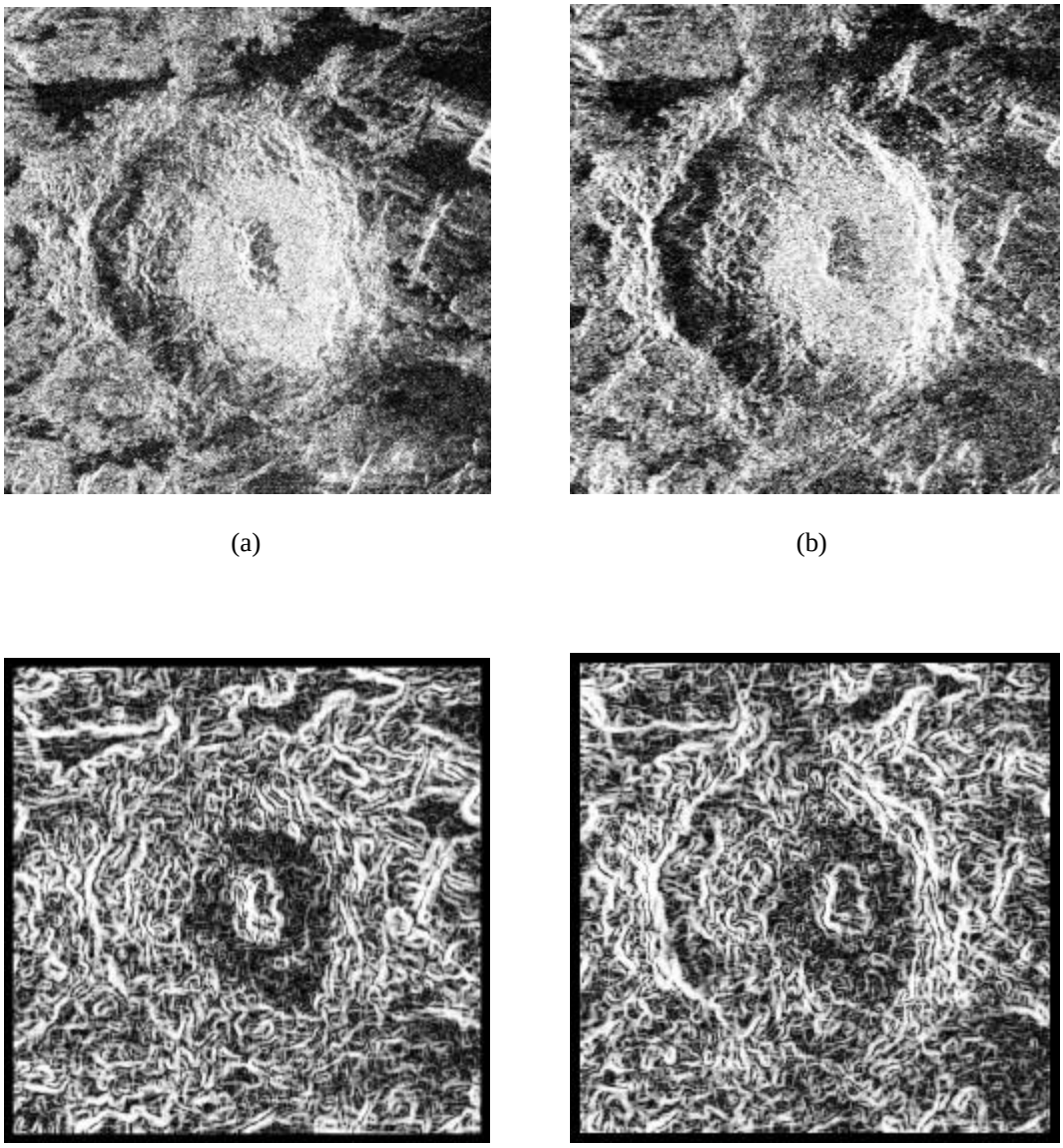

(a) (b)

(c) (d)

Fig. 5. Venusian crater as imaged by Magellan S-band SAR: (a) cycle 1 - 43.8^{o} incidence angle and (b) cycle 3 - 24.9^{o} incidence angle (the pixel size is 150m x 150m). Corresponding gradient amplitude images computed using our filter with α=1.0, ω=0.6: (c) 43.8^{o} incidence angle and (d) 24.9^{o} incidence angle.

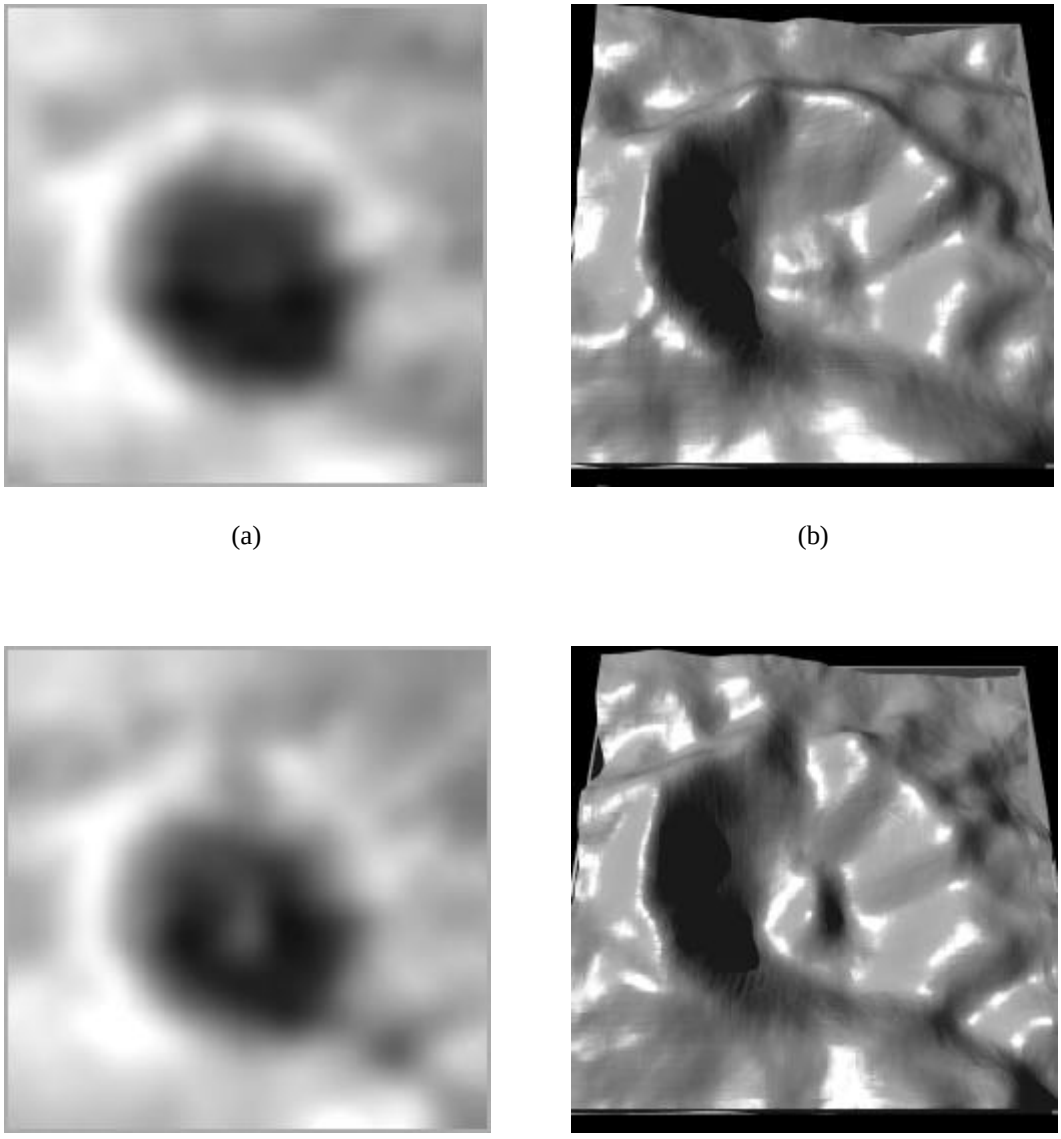

(a) (b)

(c) (d)

Fig. 6. Reconstructed DEM from initial Magellan SAR images - (a) and (b) - and from gradient amplitude images - (c) and (d).